





Testing black holes with cosmological constant in Einstein-bumblebee gravity through the black hole shadow using EHT data and deflection angle

Reggie C. Pantig ^{1,*} Shubham Kala ^{2,†} Ali Övgün ^{3,‡} and Nikko John Leo S. Lobos ^{4,§}

¹*Physics Department, Mapúa University, 658 Muralla St., Intramuros, Manila 1002, Philippines.*

²*The Institute of Mathematical Sciences, C.I.T. Campus, Taramani, Chennai 600113, India.*

³*Physics Department, Eastern Mediterranean University,
Famagusta, 99628 North Cyprus via Mersin 10, Türkiye.*

⁴*Electronics Engineering Department, University of Santo Tomas,
España Blvd, Sampaloc, Manila, 1008 Metro Manila, Philippines.*

The paper investigates black hole solutions with a cosmological constant in Einstein-Bumblebee gravity, which incorporates Lorentz symmetry breaking. Focusing on black hole thermodynamics, the study examines modifications to the first law, the equation of state, and critical points, providing insight into black hole behavior in anti-de Sitter (AdS) and de Sitter (dS) spacetimes. The presence of the bumblebee parameter is found to significantly affect black hole properties, such as the horizon radius and Hawking temperature, with larger deviations from general relativity predictions as the bumblebee parameter varies. The paper further explores black hole shadows and their potential observational constraints using Event Horizon Telescope (EHT) data. The shadow radius is influenced by both the cosmological constant and the bumblebee parameter, offering a possible avenue for testing deviations from general relativity. Additionally, weak and strong deflection angles of light near black holes in Einstein-Bumblebee gravity are computed, revealing substantial differences from standard black hole models. The study highlights how these deflection angles depend on the cosmological constant and the bumblebee parameter, emphasizing the need for highly sensitive detectors to observe such effects.

PACS numbers: 95.30.Sf, 04.70.-s, 97.60.Lf, 04.50.+h

Keywords: General relativity; Lorentz symmetry breaking; Bumblebee gravity; Black holes; Weak deflection angle; Shadow.

I. INTRODUCTION

Recently, experimental observations confirming the existence of black holes have validated a variety of theoretical frameworks conducted over the past several years [1–6]. The investigation of Lorentz symmetry violation at low energy scales, resulting from residual effects of quantum gravity at the Planck scale, has attracted considerable interest within the scientific community in recent years [7]. To investigate the potential consequences of Lorentz symmetry breaking on gravitational and cosmological phenomena, the Bumblebee model was introduced as a modified gravity theory. This model incorporates spontaneous Lorentz symmetry breaking through a Bumblebee vector field that attains a non-zero vacuum expectation value in a preferred direction [8, 9]. In Einstein-Bumblebee gravity, the interplay between the cosmological constant and the Lorentz-violating parameter offers a rich framework [10] for investigating black hole thermodynamics and optical properties. Examining these modified observables allows researchers to enhance their understanding of fundamental physics, assess the constraints of general relativity, and explore potential connections to quantum gravity.

The study of BHs thermodynamics is one of the exciting topics in the modern cosmology and astrophysical field. The first-ever relation between BHs and thermodynamics was established by Bekenstein and Hawking [11, 12]. This established the foundation for developing a semi-classical thermodynamics framework for BH solutions derived from general relativity and its recent extensions. The thermodynamics of BHs in higher-dimensional Anti-de Sitter (AdS) space has been a compelling area of research since Hawking and Page discovered a phase transition in the $(3 + 1)$ -dimensional Schwarzschild-AdS background [13]. Further, the first-order phase transition in RN-AdS black holes discovered by Chamblin in 1999 [14]. Kastor et.al. [15]. suggested that AdS BHs mass should be regarded as its enthalpy and cosmological constant is related to pressure, resulting the first law of AdS BH in extended phase space. Equation of state for rotating and higher-dimensional BHs were studied time and again and references therein [16–23]. The detailed study of criticality of charged-AdS BHs was performed by Kubiznak et.al. [24]. The thermodynamics properties of BH for three asymptotically spacetimes, flat, dS and AdS was examined by Haditale et.al. [25]. Furthermore, Jafarzade et.al [26], examined the validity of the first law of thermodynamics and the Smarr relation in the extended phase space for a AdS BH in massive gravity. More recently, Wang et.al. [27]

* rcpantig@mapua.edu.ph

† shubhamkala871@gmail.com

‡ ali.ovgun@emu.edu.tr

§ nslobos@ust.edu.ph

considered a Schwarzschild-like BH with LQG correction in spacetime under the assumption that cosmological constant is decoupled in loop quantum gravity (LQG), and investigated its thermodynamic properties in detail. The thermodynamic study of BH in Einstein-bumblebee gravity may provide an important implication for BH thermodynamics.

The black hole shadow is a dark silhouette cast by a black hole against the backdrop of bright surrounding material, typically from an accretion disk. It arises from the bending of light due to the strong gravitational field near the event horizon, as described by general relativity. These light were then describe to escape, traveling to some distant observer [28]. Then, the concept of a black hole shadow was first introduced by James Bardeen in 1973, when he studied the silhouette of a black hole as seen by a distant observer. It has been a long time since then that the fundamental equations governing the black hole shadows are known [29–33]. Progress on this topic accelerated with advancements in theoretical study [34–37] and models and computational techniques, leading to the landmark image of the supermassive black hole M87* by the Event Horizon Telescope (EHT) collaboration in 2019, which provided direct observational evidence of a black hole shadow [6, 38–41]. As it is abundant in the literature, numerous researchers have been exploring various factors affecting shadow features which may reveal possible deviations from general relativity [42–80].

One of the most fascinating phenomena arising from General Relativity (GR) is gravitational lensing (GL), in which light is bent as it passes near a compact object, such as a BH. Classical methods derived from General Relativity for calculating the deflection angle laid the foundation for later advancements in the field. Refsdal's work introduced the concept of multiple images in gravitational lensing, illustrating how gravitational fields can bend light and create several distinct images of a background source [81]. Virbhadra analyzed relativistic images formed by gravitational lensing and established methods to derive limits on the compactness of massive objects [82, 83]. In 2008, Gibbons and Werner introduced a geometrical and topological approach to investigate the gravitational deflection of light within static and spherically symmetric spacetimes, employing the GaussBonnet (GB) theorem [84]. Subsequently, Werner expanded this methodology to encompass rotating and stationary spacetimes through the application of RandersFinsler geometry [85]. Typically, most calculations utilizing the GB theorem operate under the assumption of the weak-field limit, with the receiver and source positioned at an infinite distance from the lensing object. However, in practical scenarios, both the receiver and source are invariably located at finite distances. The work of Gibbons and Werner provides a framework that enables some researchers to incorporate the finite distances of the receiver and source into the analysis of gravitational light deflection. Using the GB theorem, Ishihara et al. investigated the finite-distance deflection of light in static and spherically symmetric spacetimes, considering both weak and strong field limits [86, 87]. Thereafter, Ono et al. introduced the generalized optical metric method, applying it to analyze the finite-distance deflection angle of light in stationary, axisymmetric, and asymptotically flat spacetimes [88]. It is noteworthy that Arakida also contributed to the study of finite-distance deflection of light in static and spherically symmetric spacetimes [89]. More recently, Huang et al. presented a simplified formula for calculating the deflection angle by analyzing the double integral in the geometric expression of the deflection angle within the Gibbons-Werner method [90]. In recent years, numerous studies have leveraged the Gibbons-Werner (GW) method to investigate gravitational lensing, significantly enhancing our understanding of this phenomenon. This growing body of work has provided valuable insights into the properties of compact objects and the effects of gravitational lensing in astrophysical contexts. For a comprehensive overview, refer to the relevant literature cited herein [43, 59, 91–99].

The strong field region of a black hole holds several phenomenon that is worthy of investigation. One these phenomenon is called strong deflection angle. It calculates the amount of deflection of time-like particle as it approaches the strong field region. Bozza establish a comprehensive method in calculating the deflection angle of several black hole model [100]. The paper reveals several interesting facts. It was shown that as the light approaches the photon sphere the deflection angle diverges. There was only a certain region near the black hole SDA works. As the ratio b_0/b_{crit} deviates significantly from 1 the SDA provides non-physical results. The same methods was used in several black hole model [101–103]. In order to accommodate a more complex black hole model, Tsukamoto established a modification in order to simplify the process. The calculation on the other hand did not deviate from the original prediction of Bozza [104–106]. In this paper we investigate the behaviour of the time-like particle near black hole region of the Einstein-Bumblebee gravity model. It integrates bumblebee fields into the Einstein-Hilbert action. These bumblebee fields, characterized by a scalar-vector component, spontaneously break Lorentz symmetry and modify the structure of spacetime in ways that could be observable in astrophysical phenomena.

In GR, the deflection of light by massive objects is a well-established phenomenon, with theoretical predictions and observational confirmations providing strong support for Einsteins theory [107]. However, incorporating additional fields into gravity models, such as the bumblebee field, can significantly alter these predictions. The Einstein-Bumblebee gravity model introduces a scalar-vector field that acquires a vacuum expectation value, leading to modifications in the curvature of spacetime and consequently affecting the deflection angles of light [108]. Strong deflection angles, which represent the maximum bending of light as it approaches a massive object, are particularly sensitive to changes in spacetime geometry. Recent studies have shown that the presence of a bumblebee field can lead to deviations from GR predictions, which might be observable through astronomical observations of lensing effects [109, 110]. Investigating strong deflection angles within the Einstein-Bumblebee framework not only enhances our understanding of gravitational lensing but also provides a laboratory for evaluating the viability of modified gravity theories. By comparing theoretical predictions with observational data, researchers can probe the properties of the bumblebee field and its impact on the gravitational lensing phenomenon.

The paper is structured as follows. In Section II, we introduce the BH solution with cosmological constant in Einstein-bumblebee gravity and studied the horizon structure in detail. In Section III we investigate the black hole thermodynamics in detailed, including modified first law, equation of state and behavior of critical point. In Section IV, we examined the shadow radius and constrains our result using EHT data. The weak deflection angle and strong deflection angle is studied in Section V and VI respectively. Finally we presents the summary and conclusion in the Section VII.

II. BH WITH COSMOLOGICAL CONSTANT SPACETIME IN EINSTEIN-BUMBLEBEE GRAVITY

The metric of asymptotic flat black hole solution in Einstein-bumblebee gravity can be given as follows [111],

$$ds^2 = A(\rho)dt^2 - \frac{1+\ell}{A(\rho)}d\rho^2 - \rho^2d\Omega^2. \quad (1)$$

Here,

$$A(\rho) = 1 - \frac{2M}{\rho} - (1+\ell)\frac{\Lambda_e}{3}\rho^2, \quad (2)$$

with effective cosmological constant $\Lambda_e = k\lambda/Q$. M represents the BH mass and ℓ is the bumblebee parameter. In order to find the horizon of this BH, we solve $A(\rho) = 1 - 2M/\rho - (1+\ell)\frac{\Lambda_e}{3}\rho^2 = 0$, or equivalently the cubic equation,

$$\rho^3 - \frac{3\rho}{\Lambda_e(1+\ell)} + \frac{6M}{\Lambda_e(1+\ell)} = 0. \quad (3)$$

The solution of this cubic equation can be obtained by the usual Cardan-Tantaglia method. Based on the value of effective cosmological constant we can classified the solution.

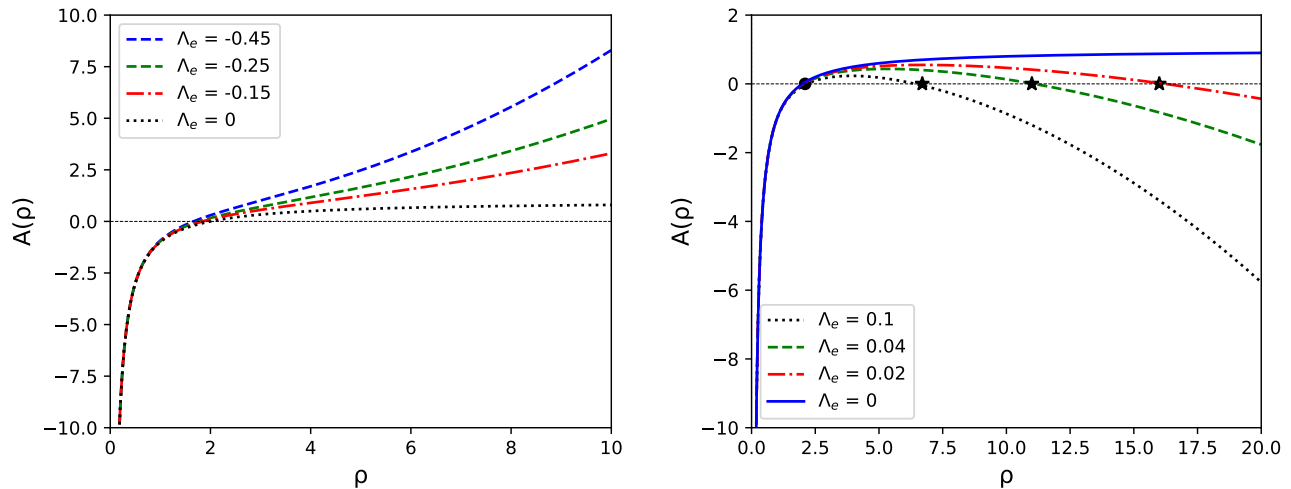


FIG. 1. The plot of $A(\rho)$ with radial distance (ρ) for AdS (left panel) and dS (right panel), with $M = 1$ and $\ell = 0.5$.

The graphical representation of $A(\rho) = 0$ is depicted in FIG.1 to understand the nature of BH horizon. It is observed that in the case of anti-de Sitter (AdS) symmetry, there exists a single horizon. However, for the de-Sitter (dS) case, there are two horizons exits. The position of the BH horizon represented by a small black circle and the cosmological horizons are depicted by a black star, respectively. Notably, it has been observed that the radius of cosmological horizon increased with an decrease in effective cosmological constant.

Case I dS ($\Lambda_e > 0$): In this case, we find the following two positive real roots,

$$\rho_{H(dS)} = \frac{2}{\sqrt{\Lambda_e(1+\ell)}} \cos \left[\frac{1}{3} \cos^{-1}(3M\sqrt{\Lambda_e(1+\ell)}) + \frac{\pi}{3} \right], \quad (4)$$

$$\rho_{C(dS)} = \frac{2}{\sqrt{\Lambda_e(1+\ell)}} \cos \left[\frac{1}{3} \cos^{-1} (3M\sqrt{\Lambda_e(1+\ell)}) - \frac{\pi}{3} \right], \quad (5)$$

Here, ρ_H and ρ_C denotes the two true horizons of the spacetime. The larger root ρ_C is known as the cosmological event horizon and the smaller root ρ_H is known as the BH event horizon. Here we consider the de Sitter geometry for which $\Lambda_e > 0$ but very small. Therefore, horizon radius can easily obtain in the limit $3M\sqrt{\Lambda_e(1+\ell)} \ll 1$. Now if we first consider $\cos \phi = x$, we have $(\frac{\pi}{2} - \phi) = \sin^{-1} x$ for $x \ll 1$. Therefore, the quantity $\cos^{-1}(3M\sqrt{\Lambda_e(1+\ell)})$ in the previous equation can be approximated with $(\frac{\pi}{2} - (3M\sqrt{\Lambda_e(1+\ell)}))$. Now, the horizon can be given as follows,

$$\rho_H \approx \frac{2}{\sqrt{\Lambda_e(1+\ell)}} \cos \left(\frac{\pi}{2} - 3M\sqrt{\Lambda_e(1+\ell)} \right) = \frac{2}{\sqrt{\Lambda_e(1+\ell)}} \sin \left(3M\sqrt{\Lambda_e(1+\ell)} \right) = 2M \left[1 + \mathcal{O}(M\sqrt{\Lambda_e(1+\ell)})^2 \right]. \quad (6)$$

The variation of BH horizon with bumblebee coupling constant (left panel) and cosmological constant (right panel) for Schwarzschild de Sitter-like case ($\Lambda_e > 0$) are depicted in FIG.2. It is observed that the effective cosmological constant and bumblebee parameter significantly increased the horizon radius. In FIG.3 we can see that the parameter ℓ may increase the event horizon and decrease the cosmological horizon for Schwarzschild-de Sitter-like case.

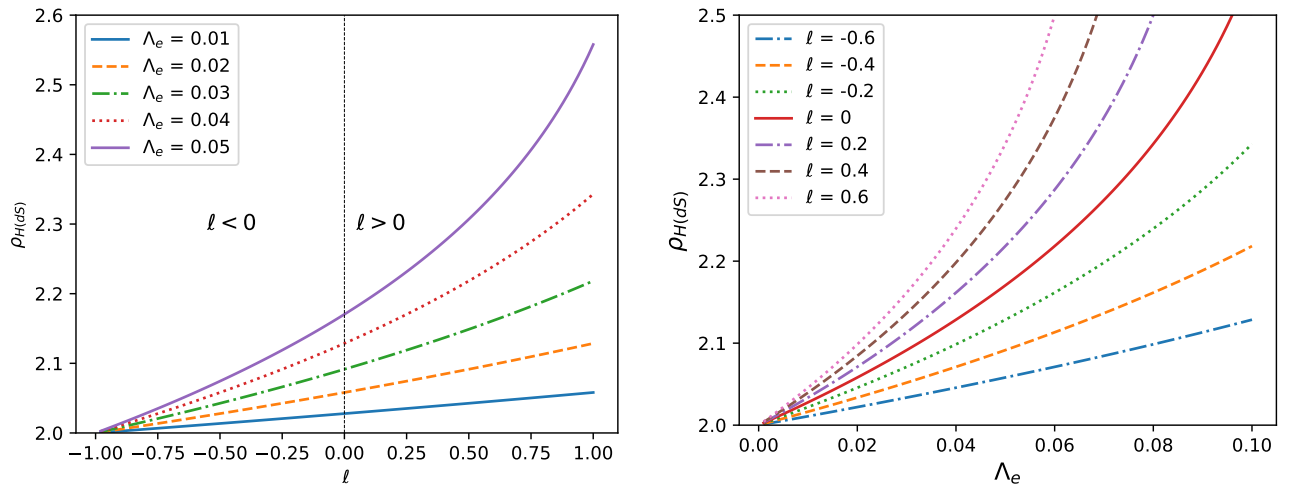


FIG. 2. The variation of BH horizon with bumblebee coupling constant (left panel) and cosmological constant (right panel) for Schwarzschild de Sitter-like case ($\Lambda_e > 0$).

Case II AdS ($\Lambda_e < 0$): In this case there is exists only a unique horizon, which radii given as,

$$\rho_{H(AdS)} = -\frac{1}{\mathcal{H}^{1/3}} - \frac{\mathcal{H}^{1/3}}{(1+\ell)\Lambda_e} \quad (7)$$

where,

$$\mathcal{H} = (1+\ell)^2 \Lambda_e^2 \left(3M + \sqrt{9M^2 - \frac{1}{(1+\ell)\Lambda_e}} \right) \quad (8)$$

The graphical representation of BH horizon for Schwarzschild anti-de Sitter-like case ($\Lambda_e < 0$) are depicted in FIG.4. It can be easily seen that horizon radius decreased with increasing the bumblebee parameter. However, the horizon radius increasing with an increase in effective cosmological constant. It is interested to observed that for $\ell < 0$ the horizon decreased exponentially and become saturated after $\ell > 0$.

III. THERMODYNAMICS OF BH WITH COSMOLOGICAL CONSTANT IN EINSTEIN-BUMBLEBEE GRAVITY

The thermodynamics of BHs is a rich and fascinating area of research which continues to yield surprises. When a cosmological constant (Λ) is included there is a natural candidate for a pressure, $P = -\frac{\Lambda}{8\pi}$ and it was proposed in [15] that

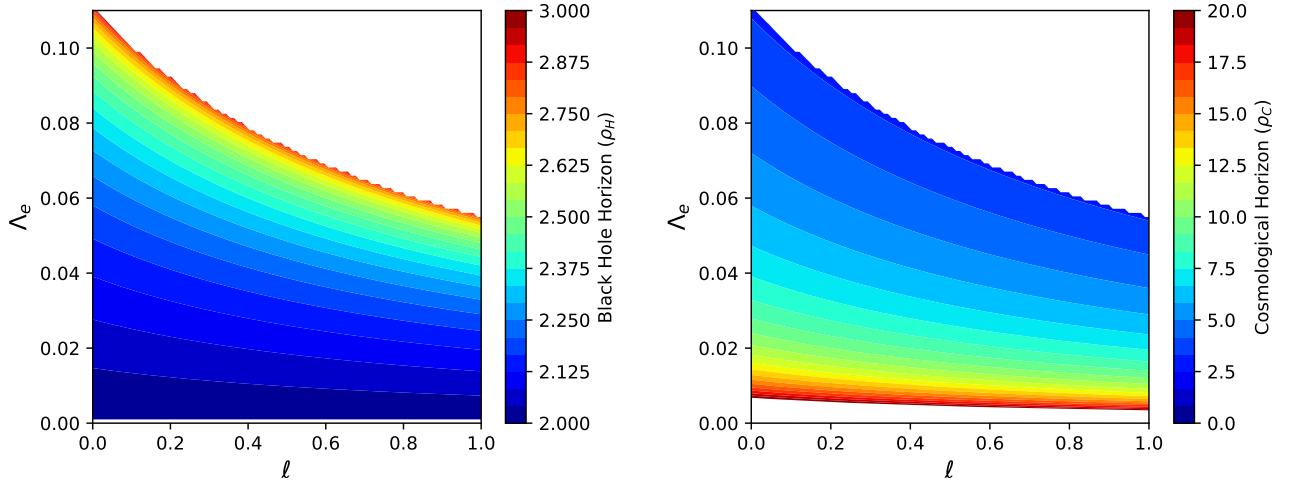


FIG. 3. The variation of black hole horizon (left panel) and cosmological horizon (right panel) with effective cosmological constant and bumblebee parameter for Schwarzschild-de Sitter-like case.

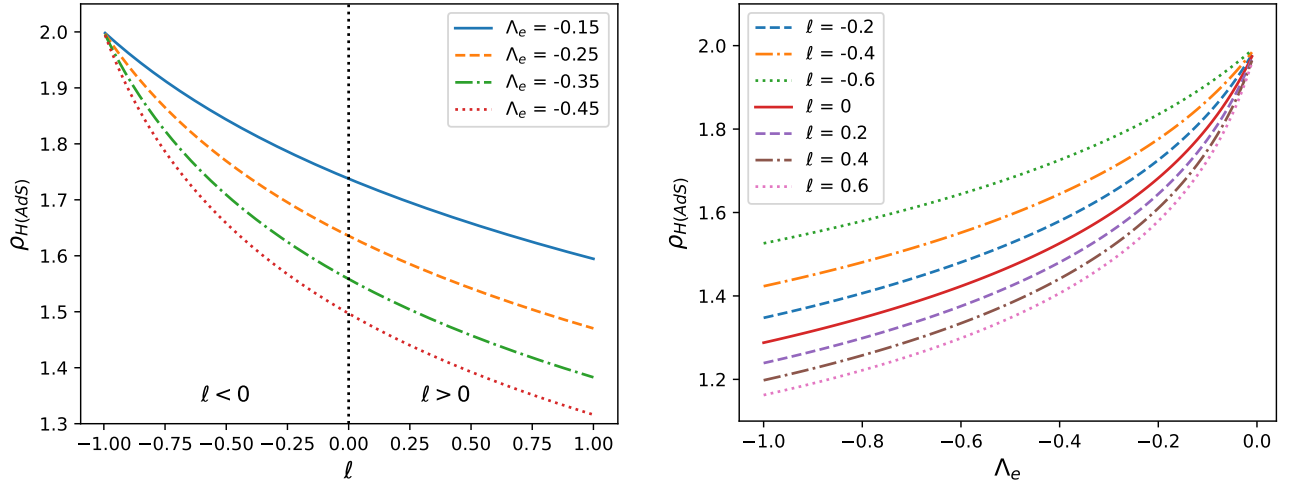


FIG. 4. The variation of BH horizon with bumblebee coupling constant (left panel) and cosmological constant (right panel) for Schwarzschild anti-de Sitter-like case ($\Lambda_e < 0$).

the volume of the BH can be defined as the thermodynamic variable conjugate to P . Interpreting the mass as the enthalpy the first law of thermodynamics can be written as,

$$dM(U) = TdS + VdP. \quad (9)$$

where the internal energy $U(S, V)$ is a function of extensive variables. The thermodynamic volume V is the conjugate variable to the pressure and is obtained from the mass, which is identified with the enthalpy $M = H(S, V)$ by

$$V = \left(\frac{\partial H}{\partial P} \right)_S. \quad (10)$$

BH event horizon play a crucial role to study the thermodynamic properties. Each event horizon has a different Hawking temperature associated with it and the system is not in thermal equilibrium. Therefore, to ensure thermal equilibrium we shall consider only the BH horizon i.e., $\Lambda_e < 0$ to study the thermodynamic properties.

The BH mass in terms of event horizon ρ_H can be obtained as follows,

$$M = \frac{\rho_H}{2} \left(1 - \frac{\Lambda_e(1+\ell)\rho_H^2}{3} \right). \quad (11)$$

and the surface gravity is,

$$\mathcal{K} = \frac{1}{2} \left(\frac{2M}{\rho_H^2} - (1-\ell) \frac{2\Lambda_e}{3} \rho_H \right). \quad (12)$$

Now the Hawking temperature could be obtained by its surface gravity as,

$$T_k = \frac{\mathcal{K}}{2\pi} = \frac{1}{4\pi} \left(\frac{2M}{\rho_H^2} - (1-\ell) \frac{2\Lambda_e}{3} \rho_H \right) \quad (13)$$

A correct description of the thermodynamics of the BH, in terms of thermodynamic potentials, requires replacing the geometric variables with thermodynamic variables. The relevant expression for the mass, and hence the enthalpy, can be written as follows,

$$H(S, P) = \frac{1}{2} \sqrt{\frac{\nu^2 S}{\pi}} \left(1 + \frac{8\nu^2 SP}{3} \right). \quad (14)$$

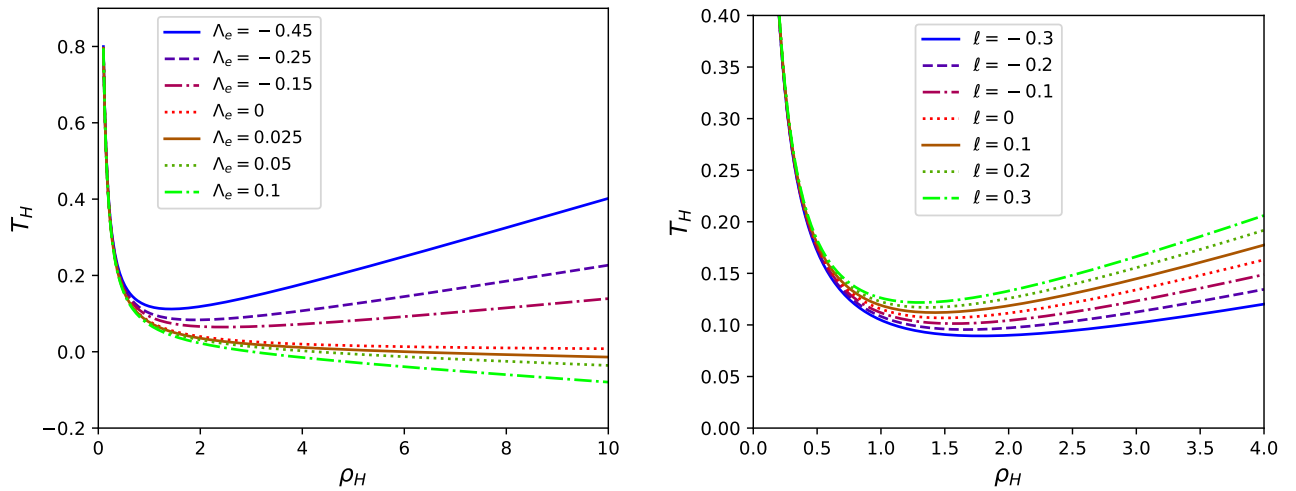


FIG. 5. The variation of BH hawking temperature with horizon radius for different values of cosmological constant (left panel) and bumblebee constant (right panel).

The usual thermodynamic relations can now be used to determine the temperature and the volume,

$$T_H = \left(\frac{\partial H}{\partial S} \right)_P = \frac{1 - \Lambda_e(1+\ell)\rho_H^2}{4\pi\rho_H}. \quad (15)$$

The temperature obtained from surface gravity is different from thermodynamic variables. The dynamics of a black hole in Einstein-Bumblebee gravity are governed by a nonlinear Lagrangian. This non-linearity is primarily due to the nonlinear potential term for the bumblebee field and the nonlinear nature of the coupling between the scalar field and the curvature in the theory. The thermodynamics of BHs solutions of non-linear electrodynamics is subtle, particularly those in which the matter Lagrangian depends on the BH mass [112]. It means that the first law of BH thermodynamics can not be applied in its simple form and some additional input is required [113].

The modified first law reads,

$$dM = TdS + VdP, \quad (16)$$

where $d\mathcal{M} = \mathcal{C}(\rho_H, \Lambda_e)$, and correction function \mathcal{C} is given as,

$$\mathcal{C} = 1 + \int_{\rho_H}^{\infty} 4\pi r^2 \frac{\partial T_0^0}{\partial M} dr, \quad (17)$$

where T_0^0 is the energy-momentum tensor which satisfy the Einstein equation. For black hole in bumblebee gravity the T_0^0 component of energy tensor momentum reads,

$$T_0^0 = \frac{1}{8\pi} \left(\frac{2M}{\rho^3} - \frac{(1-\ell)\Lambda_e}{3} \rho \right) \quad (18)$$

Therefore the correction function of the modified first law obtained as follow,

$$\mathcal{C}(\rho_H, \Lambda_e) = 1 - \frac{3(1+\ell) - (1+\ell)\Lambda_e \rho_H^2}{3\rho_H^2}. \quad (19)$$

Now we can see that the hawking temperature obtained by the modified first law is same as the temperature calculated from surface gravity. The variation of hawking temperature of BH in Einstein-bumblebee gravity is depicted in FIG.5 for different values of cosmological constant and bumblebee parameter. It has been observed that for AdS case the hawking temperature increases with decreasing the cosmological constant. The effect of bumblebee parameter on the hawking temperature made significant variation. The hawking temperature decreases for $\ell < 0$ and increases for $\ell > 0$. The largest hawking temperature achieved for the largest value of bumblebee parameter.

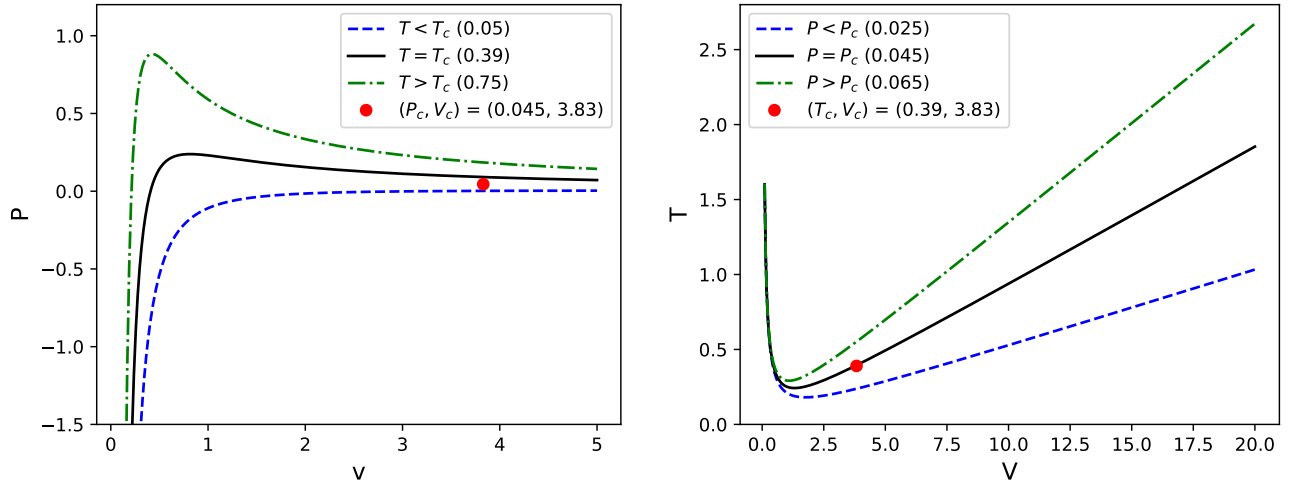


FIG. 6. P-v criticality at critical temperature (left panel) and T-v criticality at critical pressure (right panel). We consider $\ell = 0.1$ for both cases.

The entropy of the BH from modified first law given as,

$$S = \int \left(\frac{d\mathcal{M}}{T} \right)_P = \int \left(\frac{\partial \mathcal{M} / \partial \rho_H}{\partial T / \partial \rho_H} \right)_P d\rho_H = \pi \rho_H^2. \quad (20)$$

The thermodynamic volume of BH can be calculated as follows,

$$V = \left(\frac{\partial \mathcal{M}}{\partial P} \right)_S = \mathcal{C}(\rho_H, \Lambda_e) \left(\frac{\partial \mathcal{M}}{\partial P} \right)_{\rho_H} = \frac{4\pi \rho_H^3}{3}. \quad (21)$$

The expression of pressure from the condition of cosmological constant can be written as,

$$P = \frac{4\pi T_H - 1}{8\pi \rho_H (1 + \ell)}. \quad (22)$$

Here, we introduce specific volume $v = 2\rho_H$, equation of state is written as

$$P = \frac{T}{v(1+\ell)} - \frac{1}{2\pi v^2(1+\ell)}. \quad (23)$$

Now the critical point is obtained by solving the equation of state as,

$$\frac{\partial P}{\partial v} = 0, \quad \frac{\partial^2 P}{\partial v^2} = 0, \quad (24)$$

which leads to

$$P_c = \frac{1.5}{\pi^3} \left(1 - \frac{1}{2\pi(1+\ell)} \right), \quad v_c = \frac{\pi^2}{(1+\ell)} \sqrt{\frac{2}{3}}, \quad T_c = \frac{1}{\pi} \sqrt{\frac{3}{2}}. \quad (25)$$

The critical ratio is $\frac{P_c v_c}{T_c} = 0.442$. The $p-v$ criticality of BH in Einstein-bumblebee gravity provides interesting results. The critical temperature is independent from bumblebee parameter. The obtained critical ratio is slightly larger than van-der Waals ratio 0.375 (same as the RN AdS BH). Notably, the value of critical ratio observed around 3/8 for AdS BHs. However, recent studied suggest that the ration not remain constant for different alternative theories of gravity.

IV. SHADOW ANALYSIS

To determine the black hole shadow for the Schwarzschild metric, its essential to study the behavior of photons (light rays) around the black hole. Specifically, we focus on photon orbits, since the shadow is formed by the photon paths that either orbit near the black hole or are captured by it, never reaching the distant observer. A straightforward approach to this analysis is outlined in Ref. [114, 115], which we will follow here.

We review the calculation of the shadow radius in spherically symmetric space-times, where the gravitationally lensed image of a photon sphere, if present, forms the black hole shadow for an observer at infinity. Although a photon sphere often leads to a shadow, it is not strictly required for a space-time to cast one (see Ref. [116]). For a static, spherically symmetric, asymptotically flat space-time with a time-like Killing vector and diagonal metric, the line element can be expressed as

$$ds^2 = -A(\rho)dt^2 + B(\rho)d\rho^2 + C(\rho)d\Omega^2. \quad (26)$$

Here, $d\Omega$ represents the differential unit of solid angle. We define $A(\rho) = -g_{tt}(\rho)$ as the metric function and, for convenience, $C(\rho) = g_{\theta\theta} = g_{\phi\phi}/\sin^2\theta$ as the angular metric function, though this latter term is not widely used (26). In asymptotically flat space-times, $A(\rho) \rightarrow 1$ as $\rho \rightarrow \infty$, we will maintain a more general treatment for broader applicability.

We now define the function $h(\rho)$ (as introduced in, for example, Ref. [114]):

$$h(\rho) \equiv \sqrt{\frac{C(\rho)}{A(\rho)}}. \quad (27)$$

To find the radial coordinate of the photon sphere, ρ_{ph} , we solve the following implicit equation for the metric in Eq. (26).

$$\frac{d}{d\rho} [h^2(\rho_{\text{ph}})] = 0. \quad (28)$$

We can rearrange this equation into the following form:

$$C'(\rho_{\text{ph}})A(\rho_{\text{ph}}) - C(\rho_{\text{ph}})A'(\rho_{\text{ph}}) = 0. \quad (29)$$

Note that the prime represents differentiation with respect to ρ . If one takes $C(\rho) = \rho^2$, Eq. (29) simplifies to the well-known expression:

$$A(\rho_{\text{ph}}) - \frac{1}{2}\rho_{\text{ph}}A'(\rho_{\text{ph}}) = 0. \quad (30)$$

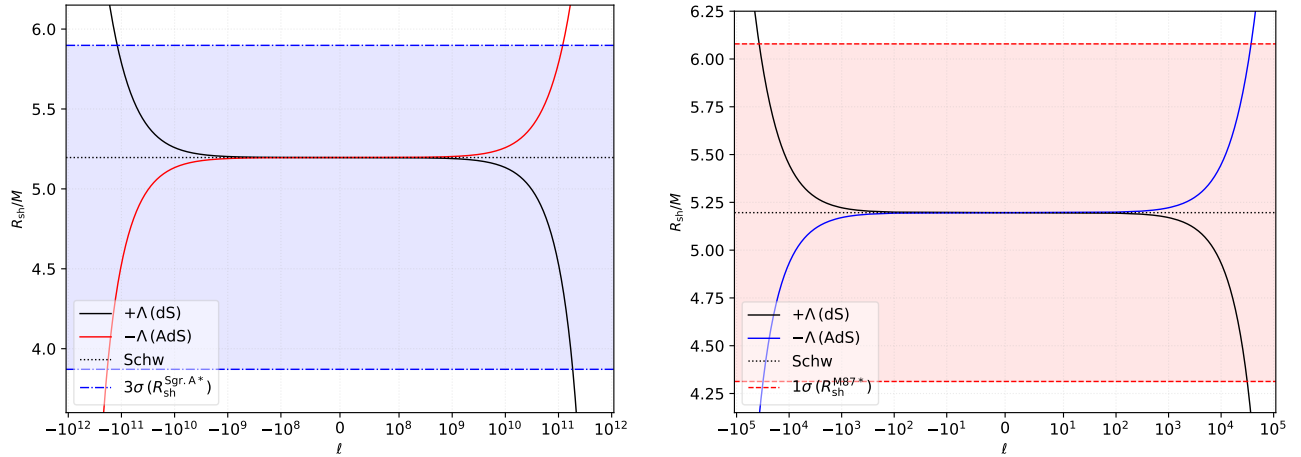


FIG. 7. Constraints for the Bumblebee parameter ℓ . Here, the accepted value of the cosmological constant Λ_e is specified in terms of the black hole mass M . In the left plot, $\Lambda_e M^2 = \pm 4.46 \times 10^{-33}$, while the right plot, $\Lambda_e M^2 = \pm 1.02 \times 10^{-26}$

The gravitational lensing of the surface at ρ_{ph} produces the shadow radius r_{sh} , which is given by (see, for example, Refs.[36, 114, 117–119]):

$$r_{\text{sh}} = \left. \sqrt{\frac{C(\rho)}{A(\rho)}} \right|_{\rho_{\text{ph}}} . \quad (31)$$

With $C(\rho) = \rho^2$ Eq. (31) becomes the shadow radius of the black hole:

$$r_{\text{sh}} = \left. \frac{\rho}{\sqrt{A(\rho)}} \right|_{\rho_{\text{ph}}} . \quad (32)$$

For the Schwarzschild black hole, shadow radius can be obtained as $r_{\text{sh}} = 3\sqrt{3}M$. This outcome is derived from the geometry of photon orbits near the black hole, with the shadow radius directly linked to the photon sphere. Furthermore, due to the high degree of spherical symmetry inherent in the Schwarzschild solution, the resulting shadow remains a perfect circle with radius r_{sh} on the image plane of a distant observer. This symmetry ensures that the shadows shape and size are unaffected by the observers inclination angle, making it independent of the viewing direction.

Due to the proximity of Sgr A*, the focus is placed on a static observer located at a distance ρ_O . In this context, the angular size of the black hole shadow, α_{sh} , is given by (see, e.g., Ref. [114]):

$$\sin^2 \alpha_{\text{sh}} = \frac{\rho_{\text{ph}}^2}{A(\rho_{\text{ph}})} \frac{A(\rho_O)}{\rho_O} . \quad (33)$$

In the physically relevant small-angle approximation, it is straightforward to observe that the shadow size is determined by:

$$r_{\text{sh}} = \rho_{\text{ph}} \sqrt{\frac{A(\rho_O)}{A(\rho_{\text{ph}})}} \sim 3\sqrt{M} - \frac{\sqrt{3}\rho_O^2(1+\ell)\Lambda_e}{2} + \mathcal{O}(M^2) . \quad (34)$$

Eq.(34) clearly shows the explicit dependence of the shadow size on the observers position. For an observer situated far from a black hole described by an asymptotically flat metric, Eq.(34) easily reduces to Eq. (32). This occurs because, at large distances, the metric function approaches $A(\rho_O) \approx 1$, as the gravitational influence of the black hole becomes negligible. Thus, when the observer is sufficiently distant, the shadow size naturally simplifies to the familiar expression.

The results from the Event Horizon Telescope (EHT) collaboration [38, 40, 115, 120] are used to constrain ℓ with the shadow radius of Sgr A* and M87*. These results are presented in Fig. 7. As noticed, there is a huge range for ℓ when we constrained it using the Sgr. A*. That is, $-10^{11} \lesssim \ell \lesssim 10^{11}$. Using the parameters for M87*, we find smaller values for the parameter: $-34311 \lesssim \ell \lesssim 34309$. Analytically, these values can be obtained through

$$\ell = - \left(1 + \frac{2\sqrt{3}\delta}{3\rho_O^2 M \Lambda_e} \right) , \quad (35)$$

where δ is the difference between r_{sh} and both the upper and lower bounds due to uncertainties. Furthermore, we see the importance and the dependence of ℓ on the position of the observer ρ_O relative to the black hole.

V. ANALYSIS OF THE DEFLECTION ANGLE IN THE WEAK FIELD LIMIT

In this section, we study the weak deflection angle of BH in Einstein-bumblebee gravity using generalized Gibbons-Werner (GW) method. Following the generalised GW method [121], we introduce the optical metric in equatorial plane $\theta = \pi/2$ to get null geodesics as follows,

$$dl^2 = \alpha_{\rho\rho}(\rho)d\rho^2 + \alpha_{\phi\phi}(\rho)d\phi^2. \quad (36)$$

The Gaussian curvature corresponding to riemannian component ($M^{\alpha 2}$) can be calculated as [85],

$$\int \mathcal{K}\sqrt{\alpha}d\rho = \int -\frac{\partial}{\partial\rho} \left(\frac{\sqrt{\alpha}}{\alpha_{\rho\rho}} \Gamma_{r\phi}^{\phi} \right) = -\frac{\alpha_{\phi\phi,\rho}}{2\sqrt{\alpha}} \quad (37)$$

As a result, the surface integration of Gaussian curvature given as,

$$\int \int_{D_\infty} \mathcal{K}ds = \int_{\phi_S}^{\phi_R} \int_{\rho_\gamma}^{\infty} \mathcal{K}\sqrt{\alpha}drd\phi. \quad (38)$$

Here, ρ_γ is the radial curvature of geodesics who along the source and observer, ϕ_S and ϕ_R are the azimuthal coordinate of source and receiver respectively. α represents the determinant of optical metric. The above expression can be written as,

$$\int \int_{D_\infty} \mathcal{K}ds = \int_{\phi_S}^{\phi_R} [H(\infty) - H(\rho_\gamma)]d\phi, \quad (39)$$

here,

$$H(\rho) = -\frac{\alpha_{\phi\phi,\rho}}{2\sqrt{\alpha}}. \quad (40)$$

On accounts of the asymptotics of $M^{\alpha 2}$, we have $H(\infty) = -1$ and the geometric expression of finite-distance deflection angle reads as [122],

$$\hat{\alpha} = \int_{\phi_S}^{\phi_R} [1 + H(\rho_\gamma)]d\phi + \int_{\gamma} kdl. \quad (41)$$

Here, k is the geodesic curvature of γ in $M^{\alpha 2}$ and can be evaluated using the following expression [123],

$$k = \frac{\beta_{\phi,\rho}}{\sqrt{\alpha\alpha^{\theta\theta}}} \quad (42)$$

For stationary BHs $\int_{\gamma} kdl = 0$ and the finite-distance deflection angle reads,

$$\hat{\alpha} = \int_{\phi_S}^{\phi_R} [1 + H(\rho_\gamma)]d\phi. \quad (43)$$

We focus on the motion of massless particles on the equatorial plane. The orbit equation can be obtained as

$$\left(\frac{du}{d\phi} \right)^2 = \frac{1}{(1+\ell)b^2} - \frac{u^2}{(1+\ell)} + \frac{2Mu^3}{(1+\ell)} + \frac{(1+\ell)\Lambda_e}{3}, \quad (44)$$

here, $u = 1/\rho$. Thus we get the perturbation solution of orbit equation as given below,

$$u = \frac{\sin \frac{\phi}{\sqrt{(1+\ell)}}}{b} + \frac{M(1 + \cos^2 \frac{\phi}{\sqrt{(1+\ell)}})}{b^2} + \frac{b\Lambda_e \sin \frac{\phi}{\sqrt{(1+\ell)}}}{6} + \frac{M\Lambda_e(1 + \cos^2 \frac{\phi}{\sqrt{(1+\ell)}})}{3} + \mathcal{O}(M^2, \Lambda_e^2), \quad (45)$$

with which we can also obtain the iterative solution of ϕ ,

$$\phi(u) = \begin{cases} \Phi(u) & \text{if } |\phi| < \frac{\pi}{2}, \\ \pi\sqrt{1+\ell} - \Phi(u) & \text{if } |\phi| \geq \frac{\pi}{2}, \end{cases} \quad (46)$$

where,

$$\begin{aligned} \Phi(u) = & \sqrt{1+\ell} \arcsin(bu) + M\sqrt{1+\ell} \frac{b^2u^2 - 2}{b\sqrt{1-b^2u^2}} - \frac{(1+\ell)\sqrt{1+\ell}\Lambda_e b}{6u\sqrt{1-b^2u^2}} + \\ & M\Lambda_e \sqrt{1+\ell} \frac{b(-3b^4u^4 + 8b^2u^2 - 4)}{6(1-b^2u^2)^{3/2}} + \mathcal{O}(M^2, \Lambda_e^2). \end{aligned} \quad (47)$$

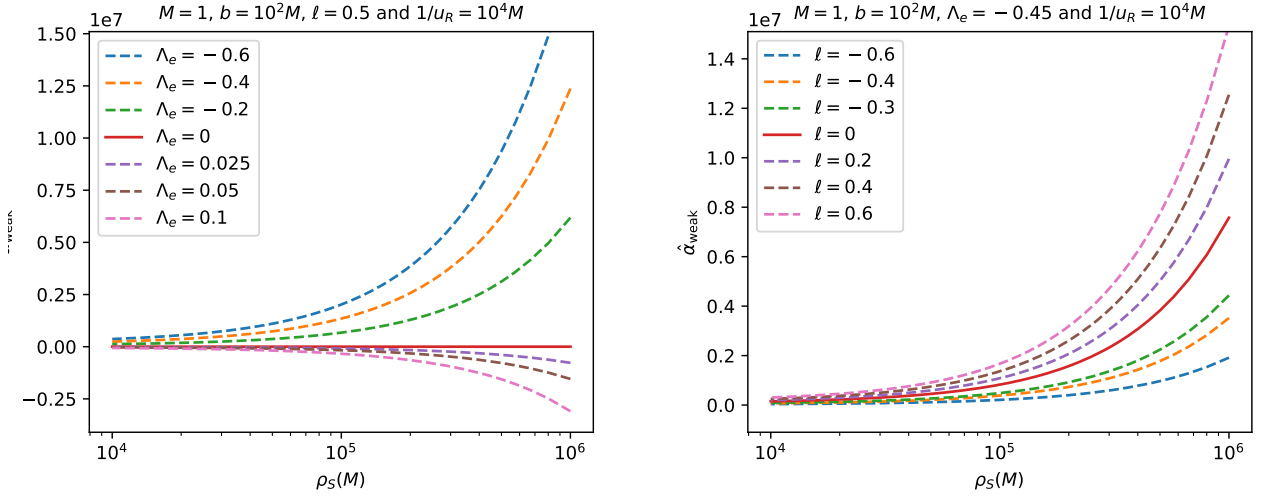


FIG. 8. The variation of deflection angle with source distance: For different values of cosmological constant (left panel) and for different values of bumblebee parameter (right panel).

Now, the optical metric of BH in Einstein-bumblebee gravity corresponding to $M^{\alpha 2}$ is given as,

$$dl^2 = \frac{(1+\ell)d\rho^2}{\left(1 - \frac{2M}{\rho} - (1-\ell)\frac{\Lambda_e}{3}\rho^2\right)^2} + \frac{\rho^2 d\phi}{1 - \frac{2M}{\rho} - (1-\ell)\frac{\Lambda_e}{3}\rho^2}. \quad (48)$$

Substituting Eq. (48) into Eq. (40) leads to,

$$H(\rho) = -\frac{1}{\sqrt{1+\ell}} + \frac{2M}{\rho\sqrt{1+\ell}} - \frac{(1+\ell)\Lambda_e\rho^2}{6\sqrt{1+\ell}} + \frac{3M^2}{\rho^2\sqrt{1+\ell}} + \frac{(1+\ell)M\Lambda_e\rho^2}{2\sqrt{1+\ell}}. \quad (49)$$

Now, from Eq. (46), we have $\phi_S = \Phi(u_S)$ and $\phi_R = \pi\sqrt{1+\ell} - \Phi(u_R)$. Therefore, using Eq. (43) the weak deflection angle is obtained as follows,

$$\begin{aligned} \hat{\alpha}_{\text{weak}} = & (\sqrt{1+\ell} - 1) [\pi - \arcsin(bu_R) - \arcsin(bu_S)] + \frac{M}{b} \left[\frac{2\sqrt{1+\ell} - b^2u_R^2(1+\sqrt{1+\ell})}{\sqrt{1-b^2u_R^2}} + \frac{2\sqrt{1+\ell} - b^2u_S^2(1+\sqrt{1+\ell})}{\sqrt{1-b^2u_S^2}} \right] \\ & - \frac{\Lambda_e b(1+\ell)\sqrt{1+\ell}}{6} \left[\frac{\sqrt{1-b^2u_R^2}}{u_R} + \frac{\sqrt{1-b^2u_S^2}}{u_S} \right] + \frac{M\Lambda_e b(1+\ell)\sqrt{1+\ell}}{6} \left[\frac{1}{\sqrt{1-b^2u_R^2}} + \frac{1}{\sqrt{1-b^2u_S^2}} \right] + \mathcal{O}(M^2, \Lambda_e^2). \end{aligned} \quad (50)$$

Here, we have used the trajectory Eq. (45) to obtain the deflection angle. The obtained expression in Eq. (50) represents the weak deflection angle of BH in bumblebee gravity. In the absence of cosmological constant, the deflection angle reduce to

the Schwarzschild-like BH in bumblebee gravity model. When $\rho_S \rightarrow b$ and $\rho_R \rightarrow b$ i.e., the source or the receiver approaches the minimum impact radius, the deflection angle will diverge. In Fig. 8, we plot the finite-deflection angle with source distance for different values of cosmological constant and bumblebee parameter. Here, we fixed $M = 1$, $b = 10^2 M$ and $\rho_R = 10^4 M$ and obtained the deflection angle in lg scale. For a fixed parameter $\ell = 0.5$, we observed that the deflection angle increases with the source distance for negative values of the cosmological constant, and the effect is more pronounced for smaller (more negative) Λ_e . Specifically, the deflection angle is stronger for smaller Λ_e . Additionally, for a fixed Λ_e , the deflection angle increases with the source distance. When comparing different values of ℓ , it was noted that the deflection angle is significantly larger for $\ell < 1$ compared to $\ell > 1$. Furthermore, the deflection angle reaches its minimum as the bumblebee parameter approaches unity.

VI. ANALYSIS OF THE DEFLECTION ANGLE IN THE STRONG FIELD LIMIT

In this section we investigate the strong deflection angle of a time-like particle in a BH in Einstein-bumblebee gravity. Extending the approach of Tsukamoto in Ref. [104] to a non-asymptotically flat black hole, the deflection angle is derived using the orbit equation shown in Eq. (44) but, in this section we express it as,

$$\left(\frac{d\rho}{d\phi}\right)^2 = \frac{R(\rho)\rho^2}{B(\rho)}, \quad (51)$$

where

$$R(\rho) = \frac{A(\rho_0)\rho^2}{A(\rho)\rho_0^2} - 1. \quad (52)$$

Note that the $A(\rho_0)$ is the metric function defined by Eq. (2), while $A(r_0)$ is the metric function evaluated at distance r_0 . The solution of Eq. (51) yields the strong deflection angle $\alpha(\rho_0)$ as shown in Ref. [100, 104]

$$\begin{aligned} \alpha(\rho_0) &= I(\rho_0) - \pi \\ &= 2 \int_{\rho_0}^{\infty} \frac{d\rho}{\sqrt{\frac{R(\rho)C(\rho)}{B(\rho)}}} - \pi. \end{aligned} \quad (53)$$

In order to evaluate the integral in Eq. (53), we expand over $\rho = \rho_0$. This yields a regular integral κ_R and a diverging integral κ_D , and by introducing a new variable, z , defined as,

$$z \equiv 1 - \frac{\rho_0}{\rho}, \quad (54)$$

$I(r_0)$ is expressed as,

$$I(\rho_0) = \int_0^1 \kappa(z, \rho_0) dz = \int_0^1 [\kappa_D(z, \rho_0) + \kappa_R(z, \rho_0)] dz, \quad (55)$$

where $\kappa(z, \rho_0)$ is expressed as the sum of the diverging integral, κ_D , and regular integral, κ_R . The details of the expansion of Eq. (53) was shown in Refs. [100, 104]. As a result the strong deflection angle is expressed as,

$$\hat{\alpha}_{\text{str}} = -\bar{a} \log\left(\frac{b_0}{b_{\text{crit}}} - 1\right) + \bar{b} + O\left(\frac{b_0}{b_c} - 1\right) \log\left(\frac{b_0}{b_c} - 1\right), \quad (56)$$

where \bar{a} and \bar{b} are coefficients of deflection angle and b_0 and b_{crit} are the impact parameter evaluated at the closest approach, ρ_0 , and critical impact parameter, respectively. The first term in Eq. (56) is the result of the diverging integral and the second term is the result of the regular integral. The coefficients \bar{a} and \bar{b} are expressed as [104],

$$\bar{a} = \sqrt{\frac{2B(\rho_{\text{ps}})A(\rho_{\text{ps}})}{2A(\rho_{\text{ps}}) - A''(\rho_{\text{ps}})\rho_{\text{ps}}^2}}, \quad (57)$$

and

$$\bar{b} = \bar{a} \log\left[\rho_{\text{ps}} \left(\frac{2}{\rho_{\text{ps}}^2} - \frac{A''(\rho_{\text{ps}})}{A(\rho_{\text{ps}})}\right)\right] + I_R(\rho_{\text{ps}}) - \pi, \quad (58)$$

where $A(\rho_{\text{ps}})$ is metric function evaluated at the photonsphere, and I_R is the regular integral evaluated from 0 to 1. The double prime in Eq. (57) and Eq. (58) correspond to the second derivative with respect to ρ evaluated over ρ_{ps} .

Evaluating the coefficients \bar{a} and the argument of the logarithmic term in \bar{b} using the equations (57) and (58), respectively, yields,

$$\begin{aligned}\bar{a} &= 1 \\ \bar{b} &= \log \left[\frac{-6}{-1 + 9\Lambda_e(\ell + 1)M^2} \right] + I_R(\rho_{\text{ps}}) - \pi.\end{aligned}\quad (59)$$

The coefficients of \bar{a} and \bar{b} are consistent with Schwarzschild strong deflection coefficient as shown in Ref. [100] when the Λ_e is reduced to zero. The regular integral I_R is defined as,

$$I_R(\rho_0) \equiv \int_0^1 f_R(z, \rho_0) - f_D(z, \rho_0) dz, \quad (60)$$

where the $f_R(z, \rho_0)$ was generated from the expansion of the trajectory in Eq. (51), which gives us

$$f_R(z, \rho_0) = \frac{2\rho_0}{\sqrt{G(z, \rho_0)}}, \quad (61)$$

where $G(z, \rho_0) = RCA(1 - z)^4$. Notice that C and A are the metric functions for which the position ρ is expressed in terms of z and ρ_0 , while R is shown in Eq. (52). The generated expression from Eq. (61) is,

$$f_R(z, \rho_{\text{ps}}) = \frac{2\rho_{\text{ps}}}{\sqrt{\sum_{m=2}^m c_m(\rho_{\text{ps}})z^m}}, \quad (62)$$

when we evaluate $\rho_0 = \rho_{\text{ps}}$. On the other hand the $f_D(z, \rho_{\text{ps}})$ is expressed as,

$$f_D(z, \rho_{\text{ps}}) = \frac{2\rho_{\text{ps}}}{\sqrt{c_2 z^2}}, \quad (63)$$

where the c 's are coefficients of the new variable z . Evaluating the integral $I_R(\rho_0)$ as $\rho_0 \rightarrow \rho_{\text{ps}}$ yields,

$$I_R(\rho_{\text{ps}}) = \ln \left(\frac{144}{(1 + \sqrt{3})^{1/4}} \right). \quad (64)$$

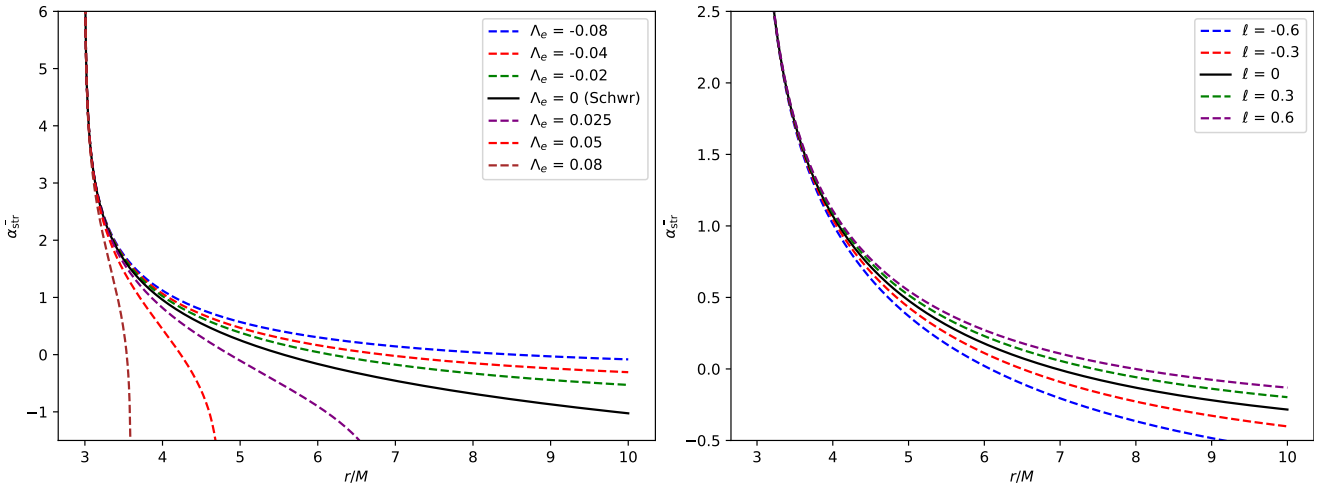


FIG. 9. The variation of strong deflection angle with respect to the closest approach, ρ_0 : For different values of cosmological constant (left panel) with $\ell = 0.05$ and for different values of bumblebee parameter (right panel) with $\Lambda = -0.045$.

The strong deflection is now expressed as,

$$\hat{\alpha}_{\text{str}} = -\log \left(\frac{b_0}{b_{\text{crit}}} - 1 \right) + \log \left[\frac{-6}{-1 + 9\Lambda_e(\ell + 1)M^2} \times \frac{144}{(1 + \sqrt{3})^{1/4}} \right] - \pi + O \left(\frac{b_0}{b_c} - 1 \right) \log \left(\frac{b_0}{b_c} - 1 \right). \quad (65)$$

To calculate the impact parameter we utilize equation ((44)) and note that $\rho \rightarrow \rho_0$ this will generate the impact parameter for the closest approach,

$$b_0^2 = \frac{-6\rho_0^3}{2\Lambda(\ell + 1)\rho_0^3 - 3\rho_0 + 3M}, \quad (66)$$

when the $\rho_0 \rightarrow 3M$ it yields the critical impact parameter.

In the strong field limit, we observe a notable dependence of the deflection angle on the bumblebee parameter, ℓ . For $\ell > 0$, the deflection angle increases proportionally with increasing ℓ . Conversely, for $\ell < 0$, the deflection angle decreases at a similar rate. For a constant value of ℓ a highly negative cosmological constant leads to an increase in the deflection angle. In contrast, when the cosmological constant becomes highly positive, we see a significant decrease in the deflection angle. Notably, the effects of a highly positive cosmological constant exhibit considerable deviation from those observed with negative values.

VII. CONCLUSIONS

In this study, we investigated the influence of the cosmological constant alongside the Bumblebee parameter on the thermodynamic and optical properties of a non-asymptotically flat black hole solution within the framework of Einstein-Bumblebee gravity. In the context of anti-de Sitter (AdS) black hole, the Hawking temperature is found to increase as the cosmological constant decreases, with notable variations due to the bumblebee parameter. Specifically, the temperature decreases for $\ell < 0$ and increases for $\ell > 0$. Additionally, the p-v criticality analysis in Einstein-Bumblebee gravity shows that the critical temperature remains independent of the bumblebee parameter, and the critical ratio slightly exceeds the van-der Waals ratio of 0.375, often approximated around 3/8 for AdS black holes.

In the weak field regime, we observed that the deflection angle increases with the source distance when the cosmological constant is negative, with more pronounced effects for smaller (more negative) values of Λ_e . Additionally, for a fixed Λ_e , the deflection angle is greater for $\ell > 0$ compared to $\ell < 0$, reaching a minimum as the bumblebee parameter approaches unity. These findings demonstrate that the deflection angle is highly sensitive to variations in both the cosmological constant and the bumblebee parameter, exhibiting significant changes based on their values and the source distance.

In the analysis of the black hole shadow within the Einstein-Bumblebee gravity framework, the study reveals intriguing modifications compared to standard general relativity predictions. The shadow radius, which serves as a crucial observational feature, is shown to be influenced by both the cosmological constant and the bumblebee parameter, ℓ . The bumblebee parameter, which reflects Lorentz symmetry breaking, alters the size of the shadow in measurable ways. Specifically, for $+\ell$, the shadow radius tends to increase. This indicates that the bumblebee parameter can either enhance or diminish the gravitational lensing effect near the black hole. Furthermore, the shadow analysis shows that these modifications are more pronounced when the cosmological constant is included. Constraints on the bumblebee parameter may be derived by comparing the observed shadow sizes of astrophysical black holes like M87* or Sgr A* with the theoretical predictions of Einstein-Bumblebee gravity. This opens the door to testing fundamental extensions of general relativity through direct astronomical observations.

As shown in Figure (9), the strong deflection angle exhibits a general increase as the position decreases, consistent with gravitational lensing behavior near compact objects. As the bumblebee parameter ℓ increases from negative to positive values, the deflection angle shifts accordingly. For $\ell > 0$, the deflection angles are higher compared to the $\ell < 0$ case, indicating that larger values of ℓ amplify the bending of light, likely due to enhanced spacetime curvature influenced by the bumblebee parameter. This suggests that the bumblebee parameter plays a significant role in modifying gravitational effects.

As the cosmological constant attains a significantly positive value, we observe a marked reduction in the deflection angle. Remarkably, the consequences associated with a highly positive cosmological constant diverge substantially from those seen with negative values, revealing profound insights into the underlying dynamics of our universe.

The effects of the cosmological constant, Λ_e , and the bumblebee parameter are coupled, leading to consistent outcomes. In the near-black hole region, where the cosmological constant is not dominant, the figure indicates that its contribution becomes detectable only when measuring the deflection angle further away from the photon sphere. A limitation of using the strong deflection angle (SDA) method is that the ratio b_0/b_{crit} must not significantly deviate from 1, necessitating the use of highly sensitive, finely-tuned detectors to observe its effects. Similarly, the influence of the bumblebee parameter becomes relevant as the particle moves away from the photon sphere. In the region where the SDA yields physical results, the impact of the bumblebee parameter requires highly sensitive astrophysical detectors to be observable.

VIII. ACKNOWLEDGEMENTS

A. Ö. and R. P. would like to acknowledge networking support of the COST Action CA21106 - COSMIC WISPerS in the Dark Universe: Theory, astrophysics and experiments (CosmicWISPerS), the COST Action CA22113 - Fundamental challenges in theoretical physics (THEORY-CHALLENGES), and the COST Action CA21136 - Addressing observational tensions in cosmology with systematics and fundamental physics (CosmoVerse).

-
- [1] A. Einstein, Sitzungsber. Preuss. Akad. Wiss. Berlin (Math. Phys.) **1915**, 844 (1915).
- [2] R. M. Wald, *General Relativity* (Chicago Univ. Pr., Chicago, USA, 1984).
- [3] S. Chandrasekhar, *The mathematical theory of black holes*, Vol. 69 (Oxford university press, 1998).
- [4] B. P. Abbott *et al.* (LIGO Scientific, Virgo), *Phys. Rev. Lett.* **116**, 061102 (2016), [arXiv:1602.03837 \[gr-qc\]](#).
- [5] R. Abbott *et al.* (LIGO Scientific, KAGRA, VIRGO), *Astrophys. J. Lett.* **915**, L5 (2021), [arXiv:2106.15163 \[astro-ph.HE\]](#).
- [6] K. Akiyama *et al.* (Event Horizon Telescope), *Astrophys. J. Lett.* **930**, L17 (2022), [arXiv:2311.09484 \[astro-ph.HE\]](#).
- [7] S. Liberati, *Class. Quant. Grav.* **30**, 133001 (2013), [arXiv:1304.5795 \[gr-qc\]](#).
- [8] V. A. Kostelecký and R. Lehnert, *Phys. Rev. D* **63**, 065008 (2001).
- [9] V. A. Kostelecký and S. Samuel, *Phys. Rev. D* **39**, 683 (1989).
- [10] R. V. Maluf and J. C. S. Neves, *Phys. Rev. D* **103**, 044002 (2021), [arXiv:2011.12841 \[gr-qc\]](#).
- [11] J. D. Bekenstein, in *JACOB BEKENSTEIN: The Conservative Revolutionary* (World Scientific, 2020) pp. 303–306.
- [12] S. W. Hawking, *Communications in mathematical physics* **43**, 199 (1975).
- [13] S. W. Hawking and D. N. Page, *Commun. Math. Phys.* **87**, 577 (1983).
- [14] A. Chamblin, R. Emparan, C. V. Johnson, and R. C. Myers, *Phys. Rev. D* **60**, 064018 (1999), [arXiv:hep-th/9902170](#).
- [15] D. Kastor, S. Ray, and J. Traschen, *Class. Quant. Grav.* **26**, 195011 (2009), [arXiv:0904.2765 \[hep-th\]](#).
- [16] R. Banerjee and D. Roychowdhury, *JHEP* **11**, 004 (2011), [arXiv:1109.2433 \[gr-qc\]](#).
- [17] S. Gunasekaran, R. B. Mann, and D. Kubiznak, *JHEP* **11**, 110 (2012), [arXiv:1208.6251 \[hep-th\]](#).
- [18] D.-C. Zou, S.-J. Zhang, and B. Wang, *Phys. Rev. D* **89**, 044002 (2014), [arXiv:1311.7299 \[hep-th\]](#).
- [19] B. P. Dolan, *Class. Quant. Grav.* **31**, 165011 (2014), [arXiv:1403.1507 \[gr-qc\]](#).
- [20] C. Promsiri, E. Hirunsirisawat, and W. Liewrian, *Phys. Rev. D* **102**, 064014 (2020), [arXiv:2003.12986 \[hep-th\]](#).
- [21] Y. Qu, J. Tao, and H. Yang, *Nucl. Phys. B* **992**, 116234 (2023), [arXiv:2211.08127 \[gr-qc\]](#).
- [22] M. S. Ali, S. G. Ghosh, and A. Wang, *Phys. Rev. D* **108**, 044045 (2023), [arXiv:2308.00489 \[gr-qc\]](#).
- [23] P. A. Cano and M. David, *JHEP* **03**, 036 (2024), [arXiv:2402.02215 \[hep-th\]](#).
- [24] D. Kubizňák and R. B. Mann, *Journal of High Energy Physics* **2012**, 1 (2012).
- [25] M. Haditale and B. Malekolkalami, *Fortschritte der Physik*, 2300267 (2023).
- [26] K. Jafarzade, B. E. Panah, and M. Rodrigues, *Classical and Quantum Gravity* **41**, 065007 (2024).
- [27] R.-B. Wang, S.-J. Ma, L. You, Y.-C. Tang, Y.-H. Feng, X.-R. Hu, and J.-B. Deng, “Thermodynamics of AdS-Schwarzschild-like black hole in loop quantum gravity,” (2024), [arXiv:2405.08241 \[gr-qc\]](#).
- [28] J. L. Synge, *Mon. Not. Roy. Astron. Soc.* **131**, 463 (1966).
- [29] J. P. Luminet, *Astron. Astrophys.* **75**, 228 (1979).
- [30] H. Falcke, F. Melia, and E. Agol, *Astrophys. J. Lett.* **528**, L13 (2000), [arXiv:astro-ph/9912263](#).
- [31] C.-M. Claudel, K. S. Virbhadra, and G. F. R. Ellis, *J. Math. Phys.* **42**, 818 (2001), [arXiv:gr-qc/0005050](#).
- [32] C. T. Cunningham and J. M. Bardeen, *Astrophys. J.* **183**, 237 (1973).
- [33] J. M. Bardeen, in *Gravitational Radiation and Gravitational Collapse*, Vol. 64, edited by C. Dewitt-Morette (1974) p. 132.
- [34] V. Dokuchaev, *Int. J. Mod. Phys. D* **28**, 1941005 (2019), [arXiv:1812.06787 \[astro-ph.HE\]](#).
- [35] V. I. Dokuchaev, N. O. Nazarova, and V. P. Smirnov, *Gen. Rel. Grav.* **51**, 81 (2019), [arXiv:1903.09594 \[astro-ph.HE\]](#).
- [36] V. I. Dokuchaev and N. O. Nazarova, *Usp. Fiz. Nauk* **190**, 627 (2020), [arXiv:1911.07695 \[gr-qc\]](#).
- [37] V. I. Dokuchaev and N. O. Nazarova, *Universe* **6**, 154 (2020), [arXiv:2007.14121 \[astro-ph.HE\]](#).
- [38] K. Akiyama *et al.* (Event Horizon Telescope), *Astrophys. J. Lett.* **875**, L1 (2019), [arXiv:1906.11238 \[astro-ph.GA\]](#).
- [39] K. Akiyama *et al.* (Event Horizon Telescope), *Astrophys. J. Lett.* **875**, L4 (2019), [arXiv:1906.11241 \[astro-ph.GA\]](#).
- [40] K. Akiyama *et al.* (Event Horizon Telescope), *Astrophys. J. Lett.* **930**, L12 (2022), [arXiv:2311.08680 \[astro-ph.HE\]](#).
- [41] K. Akiyama *et al.* (Event Horizon Telescope), *Astrophys. J. Lett.* **930**, L14 (2022), [arXiv:2311.09479 \[astro-ph.HE\]](#).
- [42] X.-J. Gao, “Gravitational lensing and shadow by a Schwarzschild-like black hole in metric-affine bumblebee gravity,” (2024), [arXiv:2409.12531 \[gr-qc\]](#).
- [43] G. Lambiase, R. C. Pantig, and A. Övgün, “Weak field deflection angle and analytical parameter estimation of the Lorentz-violating Bumblebee parameter through the black hole shadow using EHT data,” (2024), [arXiv:2408.09620 \[gr-qc\]](#).
- [44] H.-L. Li, M. Zhang, and Y.-M. Huang, *Eur. Phys. J. C* **84**, 860 (2024).
- [45] F. Atamurotov, F. Sarikulov, S. G. Ghosh, and G. Mustafa, *Phys. Dark Univ.* **46**, 101625 (2024).
- [46] H. Chen, S. H. Dong, E. Maghsoodi, S. Hassanabadi, J. Kříž, S. Zare, and H. Hassanabadi, *Eur. Phys. J. Plus* **139**, 759 (2024).
- [47] U. Papnoi, F. Atamurotov, H. Nandan, P. Pandey, G. Mustafa, and I. Saidov, *Phys. Dark Univ.* **46**, 101612 (2024).
- [48] G. D. A. Yıldız, A. Ditta, A. Ashraf, E. Güdekli, Y. M. Alanazi, and A. Reyimberganov, *Phys. Dark Univ.* **46**, 101583 (2024).
- [49] S. Zare, L. M. Nieto, X.-H. Feng, S.-H. Dong, and H. Hassanabadi, *JCAP* **08**, 041 (2024), [arXiv:2406.07300 \[astro-ph.HE\]](#).

- [50] A. Uniyal, S. Chakrabarti, R. C. Pantig, and A. Övgün, *New Astron.* **111**, 102249 (2024), [arXiv:2303.07174 \[gr-qc\]](#).
- [51] R. Alves Batista *et al.*, “White Paper and Roadmap for Quantum Gravity Phenomenology in the Multi-Messenger Era,” (2023), [arXiv:2312.00409 \[gr-qc\]](#).
- [52] R. C. Pantig, *Phys. Dark Univ.* **45**, 101550 (2024), [arXiv:2405.07531 \[gr-qc\]](#).
- [53] B. Puliçe, R. C. Pantig, A. Övgün, and D. Demir, *Fortsch. Phys.* **72**, 2300138 (2024), [arXiv:2403.02373 \[gr-qc\]](#).
- [54] N. J. L. S. Lobos, A. M. Ncube, R. C. Pantig, and A. S. Cornell, “Analyzing the effect of higher dimensions on the black hole silhouette, deflection angles, and PINN approximated quasinormal modes,” (2024), [arXiv:2406.08078 \[gr-qc\]](#).
- [55] S. Kala, H. Nandan, and P. Sharma, *Eur. Phys. J. Plus* **137**, 457 (2022), [arXiv:2207.10717 \[gr-qc\]](#).
- [56] S. Kala, Saurabh, H. Nandan, and P. Sharma, *Int. J. Mod. Phys. A* **35**, 2050177 (2020), [arXiv:2010.03615 \[gr-qc\]](#).
- [57] A. Rincon and G. Gómez, *Phys. Dark Univ.* **46**, 101576 (2024), [arXiv:2308.11756 \[gr-qc\]](#).
- [58] A. Övgün, R. C. Pantig, and A. Rincón, *Annals Phys.* **463**, 169625 (2024), [arXiv:2402.14190 \[gr-qc\]](#).
- [59] A. Övgün, R. C. Pantig, and A. Rincón, *Eur. Phys. J. Plus* **138**, 192 (2023), [arXiv:2303.01696 \[gr-qc\]](#).
- [60] A. Abdujabbarov, M. Amir, B. Ahmedov, and S. G. Ghosh, *Phys. Rev. D* **93**, 104004 (2016), [arXiv:1604.03809 \[gr-qc\]](#).
- [61] F. Atamurotov, A. Abdujabbarov, and B. Ahmedov, *Phys. Rev. D* **88**, 064004 (2013).
- [62] A. Abdujabbarov, B. Toshmatov, Z. Stuchlík, and B. Ahmedov, *Int. J. Mod. Phys. D* **26**, 1750051 (2016), [arXiv:1512.05206 \[gr-qc\]](#).
- [63] M. A. Raza, J. Rayimbaev, F. Sarikulov, M. Zubair, B. Ahmedov, and Z. Stuchlik, *Phys. Dark Univ.* **44**, 101488 (2024), [arXiv:2311.15784 \[gr-qc\]](#).
- [64] L. Chakhchi, H. El Moumni, and K. Masmar, *Phys. Dark Univ.* **44**, 101501 (2024), [arXiv:2403.09756 \[gr-qc\]](#).
- [65] L. Chakhchi, H. El Moumni, and K. Masmar, *Phys. Rev. D* **105**, 064031 (2022).
- [66] A. Belhaj, H. Belmahi, M. Benali, W. El Hadri, H. El Moumni, and E. Torrente-Lujan, *Phys. Lett. B* **812**, 136025 (2021), [arXiv:2008.13478 \[hep-th\]](#).
- [67] D. J. Gogoi, *Phys. Dark Univ.* **45**, 101535 (2024), [arXiv:2405.02455 \[gr-qc\]](#).
- [68] D. J. Gogoi and S. Ponglertsakul, *Eur. Phys. J. C* **84**, 652 (2024), [arXiv:2402.06186 \[gr-qc\]](#).
- [69] G. Lambiase, R. C. Pantig, D. J. Gogoi, and A. Övgün, *Eur. Phys. J. C* **83**, 679 (2023), [arXiv:2304.00183 \[gr-qc\]](#).
- [70] A. F. Zakharov, *Universe* **8**, 141 (2022), [arXiv:2108.01533 \[gr-qc\]](#).
- [71] A. F. Zakharov, *Phys. Rev. D* **90**, 062007 (2014), [arXiv:1407.7457 \[gr-qc\]](#).
- [72] R. A. Konoplya and A. Zhidenko, *Phys. Rev. D* **103**, 104033 (2021), [arXiv:2103.03855 \[gr-qc\]](#).
- [73] R. A. Konoplya, *Phys. Lett. B* **804**, 135363 (2020), [arXiv:1912.10582 \[gr-qc\]](#).
- [74] V. Vertogradov and A. Övgün, *Phys. Lett. B* **854**, 138758 (2024), [arXiv:2404.18536 \[gr-qc\]](#).
- [75] V. Vertogradov and A. Övgün, *Phys. Dark Univ.* **45**, 101541 (2024), [arXiv:2404.04046 \[gr-qc\]](#).
- [76] H. C. D. Lima, Junior., L. C. B. Crispino, P. V. P. Cunha, and C. A. R. Herdeiro, *Phys. Rev. D* **103**, 084040 (2021), [arXiv:2102.07034 \[gr-qc\]](#).
- [77] P. V. P. Cunha, N. A. Eiró, C. A. R. Herdeiro, and J. P. S. Lemos, *JCAP* **03**, 035 (2020), [arXiv:1912.08833 \[gr-qc\]](#).
- [78] P. V. P. Cunha, C. A. R. Herdeiro, and M. J. Rodriguez, *Phys. Rev. D* **97**, 084020 (2018), [arXiv:1802.02675 \[gr-qc\]](#).
- [79] P. V. P. Cunha, C. A. R. Herdeiro, B. Kleihaus, J. Kunz, and E. Radu, *Phys. Lett. B* **768**, 373 (2017), [arXiv:1701.00079 \[gr-qc\]](#).
- [80] N. Heidari, A. A. Araújo Filho, R. C. Pantig, and A. Övgün, “Absorption, Scattering, Geodesics, Shadows and Lensing Phenomena of Black Holes in Effective Quantum Gravity,” (2024), [arXiv:2410.08246 \[gr-qc\]](#).
- [81] S. Refsdal, *Mon. Not. Roy. Astron. Soc.* **128**, 295 (1964).
- [82] K. S. Virbhadra and G. F. R. Ellis, *Phys. Rev. D* **62**, 084003 (2000).
- [83] K. S. Virbhadra, *Phys. Rev. D* **79**, 083004 (2009).
- [84] G. W. Gibbons and M. C. Werner, *Classical and Quantum Gravity* **25**, 235009 (2008).
- [85] M. C. Werner, *Gen. Rel. Grav.* **44**, 3047 (2012), [arXiv:1205.3876 \[gr-qc\]](#).
- [86] A. Ishihara, Y. Suzuki, T. Ono, T. Kitamura, and H. Asada, *Phys. Rev. D* **94**, 084015 (2016).
- [87] A. Ishihara, Y. Suzuki, T. Ono, and H. Asada, *Phys. Rev. D* **95**, 044017 (2017).
- [88] T. Ono, A. Ishihara, and H. Asada, *Phys. Rev. D* **98**, 044047 (2018).
- [89] H. Arakida, *Gen. Rel. Grav.* **50**, 48 (2018), [arXiv:1708.04011 \[gr-qc\]](#).
- [90] Y. Huang, Z. Cao, and Z. Lu, *Journal of Cosmology and Astroparticle Physics* **2024**, 013 (2024).
- [91] K. Jusufi, M. C. Werner, A. Banerjee, and A. Övgün, *Phys. Rev. D* **95**, 104012 (2017).
- [92] K. Jusufi and A. Övgün, *Phys. Rev. D* **97**, 024042 (2018).
- [93] A. Övgün, *Phys. Rev. D* **98**, 044033 (2018).
- [94] Z. Li and A. Övgün, *Phys. Rev. D* **101**, 024040 (2020).
- [95] R. C. Pantig, L. Mastrototaro, G. Lambiase, and A. Övgün, *Eur. Phys. J. C* **82**, 1155 (2022), [arXiv:2208.06664 \[gr-qc\]](#).
- [96] R. C. Pantig and A. Övgün, *Annals Phys.* **448**, 169197 (2023), [arXiv:2206.02161 \[gr-qc\]](#).
- [97] A. Rincón, A. Övgün, and R. C. Pantig, *Phys. Dark Univ.* **46**, 101623 (2024), [arXiv:2409.10930 \[gr-qc\]](#).
- [98] W. Javed, M. Atique, R. C. Pantig, and A. Övgün, *Symmetry* **15**, 148 (2023), [arXiv:2301.01855 \[gr-qc\]](#).
- [99] R. C. Pantig, “On the analytic generalization of particle deflection in the weak field regime and shadow size in light of EHT constraints for Schwarzschild-like black hole solutions,” (2024), [arXiv:2409.00476 \[gr-qc\]](#).
- [100] V. Bozza, *Physical Review D* **66**, 103001 (2002).
- [101] R. Cavalcanti, A. G. Da Silva, and R. Da Rocha, *Classical and Quantum Gravity* **33**, 215007 (2016).
- [102] G. Abbas, A. Mahmood, and M. Zubair, *Physics of the Dark Universe* **31**, 100750 (2021).
- [103] I. N. Huda and H. S. Ramadhan, *J. Phys. Conf. Ser.* **1816**, 012021 (2021).

- [104] N. Tsukamoto, *Physical Review D* **95**, 064035 (2017).
- [105] N. Tsukamoto, *Physical Review D* **102**, 104029 (2020).
- [106] N. Tsukamoto, *Physical Review D* **103**, 024033 (2021).
- [107] A. Einstein, *Science* **84**, 506 (1936).
- [108] F. Poulis and M. Soares, *The European Physical Journal C* **82**, 1 (2022).
- [109] Í. D. Carvalho, G. Alencar, W. Mendes, and R. Landim, *Europhysics Letters* **134**, 51001 (2021).
- [110] W. Javed, T. Zahra, R. C. Pantig, and A. Övgün, "Light Deflection by Traversable Wormhole in Einstein-Bumblebee Gravity with an Antisymmetric Tensor," (2023).
- [111] C. Ding, C. Liu, Y. Xiao, and J. Chen, "Phantom black holes and wormholes in Einstein-bumblebee gravity," (2024), [arXiv:2407.16916 \[gr-qc\]](https://arxiv.org/abs/2407.16916).
- [112] M.-S. Ma and R. Zhao, *Class. Quant. Grav.* **31**, 245014 (2014), [arXiv:1411.0833 \[gr-qc\]](https://arxiv.org/abs/1411.0833).
- [113] Y. Zhang and S. Gao, *Class. Quant. Grav.* **35**, 145007 (2018), [arXiv:1610.01237 \[gr-qc\]](https://arxiv.org/abs/1610.01237).
- [114] V. Perlick and O. Y. Tsupko, *Phys. Rept.* **947**, 1 (2022), [arXiv:2105.07101 \[gr-qc\]](https://arxiv.org/abs/2105.07101).
- [115] S. Vagnozzi *et al.*, *Class. Quant. Grav.* **40**, 165007 (2023), [arXiv:2205.07787 \[gr-qc\]](https://arxiv.org/abs/2205.07787).
- [116] A. B. Joshi, D. Dey, P. S. Joshi, and P. Bambhaniya, *Phys. Rev. D* **102**, 024022 (2020), [arXiv:2004.06525 \[gr-qc\]](https://arxiv.org/abs/2004.06525).
- [117] D. Psaltis, *Phys. Rev. D* **77**, 064006 (2008), [arXiv:0704.2426 \[astro-ph\]](https://arxiv.org/abs/0704.2426).
- [118] P. V. P. Cunha and C. A. R. Herdeiro, *Gen. Rel. Grav.* **50**, 42 (2018), [arXiv:1801.00860 \[gr-qc\]](https://arxiv.org/abs/1801.00860).
- [119] D. Psaltis *et al.* (Event Horizon Telescope), *Phys. Rev. Lett.* **125**, 141104 (2020), [arXiv:2010.01055 \[gr-qc\]](https://arxiv.org/abs/2010.01055).
- [120] P. Kocherlakota *et al.* (Event Horizon Telescope), *Phys. Rev. D* **103**, 104047 (2021), [arXiv:2105.09343 \[gr-qc\]](https://arxiv.org/abs/2105.09343).
- [121] Y. Huang, Z. Cao, and Z. Lu, *JCAP* **01**, 013 (2024), [arXiv:2306.04145 \[gr-qc\]](https://arxiv.org/abs/2306.04145).
- [122] Y. Huang and Z. Cao, *Eur. Phys. J. C* **83**, 80 (2023), [arXiv:2212.04254 \[gr-qc\]](https://arxiv.org/abs/2212.04254).
- [123] T. Ono, A. Ishihara, and H. Asada, *Phys. Rev. D* **96**, 104037 (2017).